Calcif Tissue Int (2011) 89:10–20
DOI 10.1007/s00223-011-9487-z

ORIGINAL RESEARCH

Mineral Composition is Altered by Osteoblast Expression of an Engineered G_s-Coupled Receptor

G. J. Kazakia · D. Speer · S. Shanbhag · S. Majumdar · B. R. Conklin · R. A. Nissenson · E. C. Hsiao

Received: 28 December 2010 / Accepted: 6 March 2011 / Published online: 28 April 2011

Abstract Activation of the G_s G protein–coupled receptor Rs1 in osteoblasts increases bone mineral density by 5- to 15-fold in mice and recapitulates histologic aspects of fibrous dysplasia of the bone. However, the effects of constitutive G_s signaling on bone tissue quality are not known. The goal of this study was to determine bone tissue quality in mice resulting from osteoblast-specific constitutive G_s activation, by the complementary techniques of FTIR spectroscopy and synchrotron radiation micro-computed tomography (SRμCT). Col1(2.3)-tTA/TetO-Rs1 double transgenic (DT) mice, which showed osteoblast-specific constitutive G_s signaling activity by the Rs1 receptor, were created. Femora and calvariae of DT and wild-type (WT) mice (6 and 15 weeks old) were analyzed by FTIR spectroscopy. WT and DT femora (3 and 9 weeks old) were imaged by SRμCT. Mineral-to-matrix ratio was 25% lower ($P = 0.010$), carbonate-to-phosphate ratio was 20% higher ($P = 0.025$), crystallinity was 4% lower ($P = 0.004$), and cross-link ratio was 11% lower ($P = 0.025$) in 6-week DT bone. Differences persisted in 15-week animals. Quantitative SRμCT analysis revealed substantial differences in mean values and heterogeneity of tissue mineral density (TMD). TMD values were 1,156 ± 100 and 711 ± 251 mg/cm^3 (mean ± SD) in WT and DT femoral diaphyses, respectively, at 3 weeks. Similar differences were found in 9-week animals. These results demonstrate that continuous G_s activation in murine osteoblasts leads to deposition of immature bone tissue with reduced mineralization. Our findings suggest that bone tissue quality may be an important contributor to increased fracture risk in fibrous dysplasia patients.

Keywords Fourier transform infrared spectroscopy · Synchrotron micro-computed tomography · Bone formation · Bone quality · Mineralization · G_s signaling · Rs1 transgenic mice · Receptors activated solely by synthetic ligands (RASSLs) · G protein–coupled receptors · Fibrous dysplasia of bone

The authors have stated that they have no conflict of interest.

G. J. Kazakia (✉) · S. Majumdar
Musculoskeletal Quantitative Imaging Research Group, Department of Radiology and Biomedical Imaging, University of California, San Francisco, 185 Berry St., Suite 350, San Francisco, CA 94107, USA
e-mail: galateia.kazakia@ucsf.edu

D. Speer · S. Shanbhag
University of California, Berkeley, CA, USA

B. R. Conklin · E. C. Hsiao
Gladstone Institute of Cardiovascular Disease, San Francisco, CA, USA

B. R. Conklin · R. A. Nissenson · E. C. Hsiao
Department of Medicine, University of California, San Francisco, CA, USA

R. A. Nissenson
Endocrine Research Unit, Veterans Affairs Medical Center, San Francisco, CA, USA

Osteoblast G protein–coupled receptors (GPCRs) are fundamental regulators of skeletal maintenance and repair. Activation of osteoblast G_s-GPCR signaling increases bone mass, as in pathological conditions such as fibrous dysplasia of the bone and McCune-Albright syndrome [1, 2]. However, the affected bone is associated with increased fragility. In contrast, intermittent activation of the parathyroid hormone receptor (PTH1R) by recombinant parathyroid hormone (teriparatide) [3] increases bone

formation and is an important treatment for osteoporosis. Manipulation of skeletal GPCR signaling, therefore, is a potentially potent technique for regulating disease processes and enhancing repair of bone tissue [4].

The skeletal effects of G_s-GPCR signaling on bone formation were investigated with the Col1(2.3)-tTA/TetO-Rs1 mouse model of fibrous dysplasia of the bone. This model uses a synthetic biology approach [4] to activate the G_s signaling pathway in maturing mouse osteoblasts by the constitutive G_s activity of the Rs1 engineered receptor activated solely by a synthetic ligand (RASSL) [5, 6]. RASSLs are engineered receptors that no longer respond to endogenous hormones but are activated by synthetic small-molecule drugs. They have been useful for studying the roles of G-protein signaling in a variety of in vivo systems [7–10]. In the Col1(2.3)-tTA/TetO-Rs1 mouse model, Rs1 expression was sufficient to induce a dramatic increase in skeletal bone mass and trabecular bone formation [6]. In addition, cortical bone was lost, the normal bone marrow canal was obliterated, and the normal bone marrow cellular components were replaced by a large number of small cells that histologically resemble young osteoblasts. These features show strong similarity to the bony lesions in patients with fibrous dysplasia of the bone, a disease that also results from activation of the G_s signaling pathway [1, 2].

While elevated osteoblast G_s signaling has significant effects on bone mass and structure, the quality of the resulting bone tissue has not been thoroughly investigated. Characteristics of bone tissue quality, including mineral content and composition, crystal size and perfection, and collagen matrix stability, are critical to the mechanical competence [11–14] and remodeling characteristics [15, 16] of bone. Therefore, evaluation of tissue quality metrics is crucial for understanding the anabolic effect of constitutive G_s signaling on bone and for developing effective treatments for skeletal pathology.

We applied two complementary strategies for assessing bone quality in mice with osteoblast-specific constitutive G_s signaling activity: Fourier transform infrared (FTIR) spectroscopy, to investigate tissue quality at the molecular level, and synchrotron radiation micro-computed tomography (SRμCT), to provide accurate quantification of bone tissue mineral density (TMD) at high spatial resolution.

FTIR spectroscopy provides a method for examining tissue quality and composition by measuring molecular bond vibration frequencies [17, 18]. FTIR spectra of calcified tissues typically provide information on the structure and environment of the carbonate and phosphate groups of the mineral phase and the amide groups of the organic matrix. Metrics of bone quality can be calculated from these data. Specifically, these parameters include mineral-to-matrix ratio (correlated to ash density [19, 20]), carbonate-to-phosphate ratio (reflecting the level of carbonate substitution into the apatite lattice [15, 21]), crystallinity (related to crystal size and perfection as determined by X-ray diffraction [22, 23]), and collagen cross-link ratio (the ratio of nonreducible to reducible cross-links, indicating collagen maturity and stability [24]). These FTIR parameters provide information on the structure and mineralization of the inorganic and organic components of bone.

SRμCT enables accurate TMD quantification at high spatial resolution. In this technique, a high photon flux monochromatic X-ray beam extracted from a synchrotron beam replaces the standard polychromatic X-ray beam used in conventional μCT devices. The use of a single X-ray beam energy eliminates beam-hardening artifacts, the high photon flux produces a high signal-to-noise ratio and high spatial resolution, and the use of a nearly parallel beam enables exact 3D tomographic reconstruction. Due to these factors, TMD quantification by SRμCT is more accurate than that by conventional μCT. SRμCT TMD assessment has been verified against gravimetric methods (ashing) [25] and 2D microradiography [26] and is currently considered the gold standard for high-resolution 3D TMD evaluation.

In this study, we used FTIR spectroscopy and SRμCT to evaluate measures of bone tissue mineralization, composition, and maturity in mice with osteoblast-specific constitutive G_s signaling activity. Our results show that the bone formed by activated G_s signaling is more immature and has lower mineralization than that of wild-type (WT) controls. These findings suggest that reduced bone quality contributes to increased bone fragility in fibrous dysplasia patients. In addition, our results illustrate that metrics of bone tissue quality are important in investigating signaling mechanisms.

Materials and Methods

Mouse Model

All transgenic mouse studies were approved by and performed in accordance with the Institutional Animal Care and Use Committee and the Laboratory Animal Research Center at the University of California, San Francisco. ColI(2.3)-tTA/TetO-Rs1 double transgenic (DT) mice were generated by heterozygote crosses of mice carrying the TetO-Rs1 transgene [6] with mice carrying the ColI(2.3)-tTA transgene [27], as described [6]. Transgene expression was activated by maintaining the mice on regular mouse chow without doxycycline (LabDiet 5053; PMI Nutrition, St. Louis, MO). These transgenic mice display osteoblast-specific constitutive G_s signaling activity through the Rs1 receptor. Previous qPCR assays on whole femora of 6-week-old adult mice showed that Rs1 expression was

selectively and highly induced in the bones of DT mice [6]. All studies compared DT mice to WT littermate controls.

FTIR Spectroscopy

Femora and calvariae of DT and WT mice were analyzed by FTIR spectroscopy. Mice of two ages were evaluated: 6 weeks ($n = 6$ WT, 6 DT) and 15 weeks ($n = 6$ WT, 6 DT). Bones were excised, stripped of soft tissue, and fixed in 70% ethanol. The desired region of each specimen was isolated and desiccated through an ethanol series, followed by exposure in a desiccant chamber. The sampled regions were the mid-diaphysis of the left femur and the left posterior quadrant (parietal bone) of the calvaria (Fig. 1). For each sample, a 2-mg (approximately 2 mm long) bone segment was isolated and a homogenized powder mixture was created of 1% bone by weight in potassium bromide (KBr; Thermo Electron, Waltham, MA). The powder mixture was compressed using a manual die to create a pellet for FTIR spectroscopy.

Spectroscopy was performed on a benchtop interferometer system (Nexus 870, Thermo Electron). Spectra were acquired using 256 scans at a spectral resolution of 4 cm^{-1}. A background scan was recorded immediately after each sample scan to facilitate background correction. After acquisition, the spectra were transferred to chemical imaging software (Isys; Spectral Dimensions, Olney, MD) for analysis. Spectra were baseline-adjusted and the integrated areas of the amide I (1,595–1,720 cm^{-1}), $\nu_1\nu_3$ phosphate (PO_4^{3-}, 895–1,215 cm^{-1}), and ν_2 carbonate (CO_3^{2-}, 840–890 cm^{-1}) bands were calculated. Mineral-to-matrix (PO_4^{3-}/amide I), carbonate-to-phosphate (CO_3^{2-}/PO_4^{3-}), and carbonate-to-matrix (CO_3^{2-}/amide I) ratios were calculated from integrated areas of the respective peaks. Additionally, peak heights were measured at specific wave numbers: 1,020, 1,030, 1,660, and 1,690 cm^{-1}. From these, a series of absorbance ratios were calculated to determine additional spectroscopic parameters. The ratio of 1,030 to 1,020 cm^{-1} represents the ratio of stoichiometric apatite to nonstoichiometric apatite, a measure of crystallinity. Finally, the ratio of 1,660 to 1,690 cm^{-1} represents the proportion of nonreducible to reducible cross-links in the collagen, indicative of collagen maturity.

FTIR Spectroscopy—Repeatability

Left femora from each of three 15-week-old WT mice were used to assess repeatability of FTIR measures. From each femur, a mid-diaphyseal section was isolated and processed into a homogeneous powder mixture of 1% bone by weight in KBr as described above. Three pellets were created from each batch of the homogenized mixture, and the remaining powder was stored in the desiccator to prevent hydration

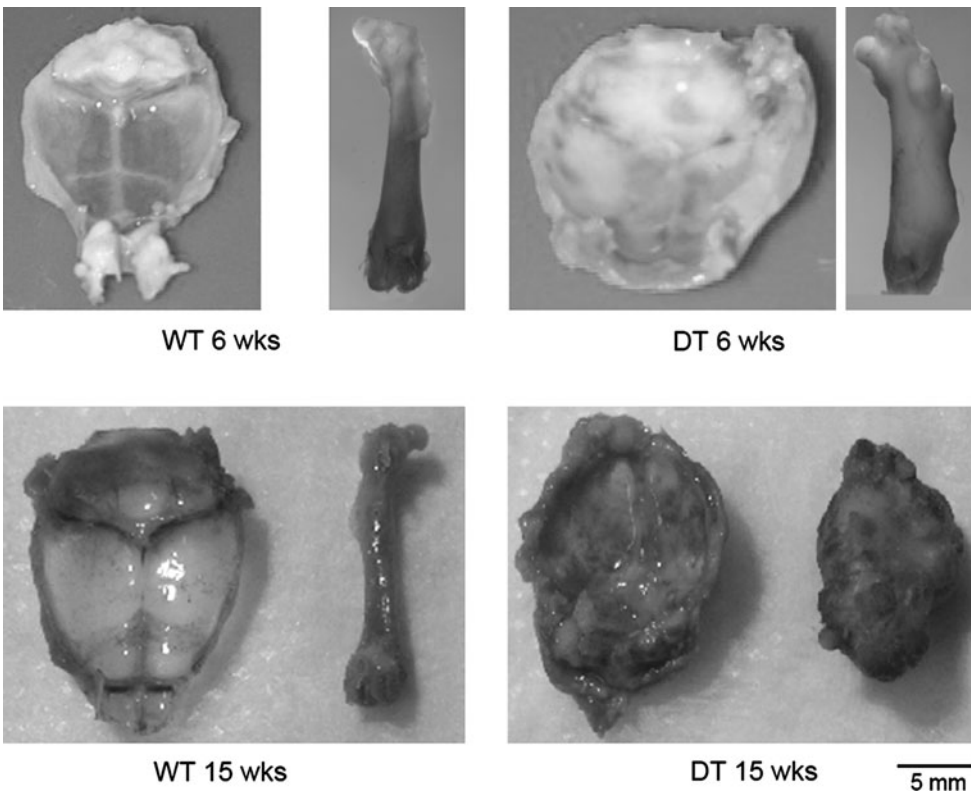

Fig. 1 Calvariae and femora of representative wild-type (*WT*) and double transgenic (*DT*) mice harvested at 6 and 15 weeks of age for FTIR analysis. DT mice exhibited increased femoral girth and calvarial thickness at 6 weeks, becoming more dramatic at 15 weeks. *Scale bar* 5 mm for each image

between each pellet preparation. Spectroscopy and analysis of the three pellets from each bone were performed consecutively on a single day, following the methods detailed in the previous section.

Synchrotron μCT Imaging

One representative femur from 3- and 9-week-old WT and DT mice was imaged using SRμCT. Femora were dissected, stripped of soft tissue, fixed in 10% neutral buffered formalin for 24 h, and stored in 70% ethanol before imaging. The distal surface of the femoral condyles was mounted onto a block for imaging with a wax-based adhesive. Synchrotron imaging was performed at the European Synchrotron Radiation Facility (Grenoble, France). Beamline ID19 of this facility is equipped with a μCT acquisition system capable of producing high-resolution 3D images with high contrast and signal-to-noise ratio [28]. Images were acquired using a single energy (21 keV) chosen to provide suitable contrast. The transmitted monochromatic X-ray beam was recorded using a scintillator coupled to a 2D 1,024 × 1,024 charge coupled device (CCD) camera. The optical system was arranged to produce a pixel size of 5 μm. Dark current and reference images without the specimen were taken during acquisition for flat field correction. Three-dimensional images were reconstructed by means of a 3D filtered back-projection algorithm from 900 projections. A local thresholding scheme [29] was employed to segment the bone from background (Fig. 2). This local thresholding scheme was necessitated by the variations in voxel intensity observed in the synchrotron images; global thresholds failed to capture the entire mineralized region, particularly in DT bone, and therefore underestimated TMD variation and miscalculated mean TMD. After segmentation, average linear attenuation was calculated and directly converted to TMD with a theoretical relationship modeling linear attenuation coefficient as a function of hydroxyapatite concentration.

DXA Analysis

Whole-body DXA scans of WT and DT mice were performed for animals aged 3 weeks ($n = 10$ WT, 14 DT), 6 weeks ($n = 10$ WT, 10 DT), 9 weeks ($n = 8$ WT, 14 DT), and 15 weeks ($n = 7$ WT, 7 DT) to assess phenotype progression. Whole-body DXA scans were performed under anesthesia with 1% isoflurane in a Lunar PIXImus2 (GE Lunar, Waukesha, WI), as described previously [6].

Histology

Femora of 6-week-old DT and WT mice collected for histology were fixed in 10% neutral buffered formalin for 24 h. Undecalcified femora were embedded in polymethyl methacrylate [6], and 4-μ sections were cut on a hard-tissue microtome. Decalcified bones were processed in 10% EDTA, embedded in paraffin, sectioned, and stained with hematoxylin and eosin (H&E) by the Gladstone Institutes Histology Core (San Francisco, CA). Mid-diaphyseal regions of interest were visualized to grossly assess phenotypic changes.

Statistics

Wilcoxon signed-rank tests revealed no significant differences in FTIR spectroscopic parameters between the two anatomic sites (femur, calvaria); therefore, values were averaged to produce a single result per animal. Results obtained from WT and DT mouse specimens were compared using *t*-tests or Wilcoxon rank sums tests as appropriate. Repeatability of FTIR measures was determined by calculating the coefficient of variation (CV) for each

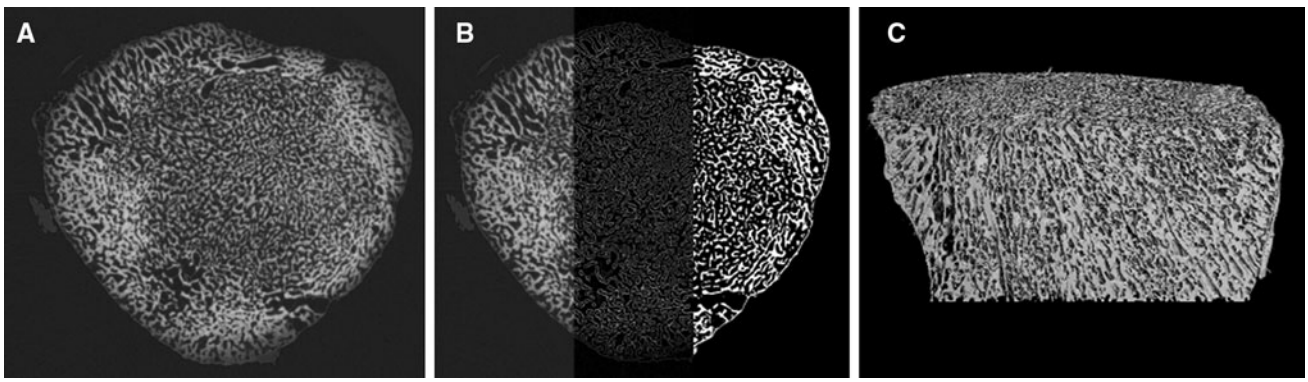

Fig. 2 Mid-diaphyseal femoral cross section of a 3-week-old double transgenic mouse. Gray-scale data (**a**) were processed using a local thresholding algorithm that incorporates edge detection (**b**, *center panel* shows result of edge detection), allowing accurate segmentation (**b**, *right panel* shows result of segmentation) despite the existence of fine structures and dramatic spatial variation in attenuation. A rendering of the resulting 3D segmented data set is shown (**c**)

femoral specimen, then computing mean CV for the three femora used in the repeatability study.

Results

FTIR Spectroscopy

FTIR spectroscopy was performed to assess bone quality in young (6 weeks) and mature (15 weeks) WT and DT mice. No differences in FTIR spectroscopic parameters were detected between the two anatomic sites we tested (femora and calvaria) for either WT or DT animals, despite the different bone-formation processes (endochondral vs. intramembranous) represented by the two sites.

Significant differences in FTIR spectroscopic measures of bone composition were found between 6-week-old WT and DT mice (Table 1, Fig. 3). Mineral-to-matrix ratio was 25% lower in DT bone ($P = 0.010$), carbonate-to-phosphate ratio was 20% higher ($P = 0.025$), crystallinity was 4% lower ($P = 0.004$), and cross-link ratio was 11% lower ($P = 0.025$). These differences persisted in 15-week-old animals. No differences were found between WT and DT mice in carbonate-to-matrix ratio ($P = 0.084$ at 6 weeks, $P = 0.107$ at 15 weeks). Differences associated with animal age were detected only in WT mice. WT carbonate-to-phosphate ratio increased 17% from 6 to 15 weeks ($P = 0.017$), carbonate-to-matrix ratio increased 49% ($P = 0.007$), and cross-link ratio decreased 8% ($P = 0.037$). Change in carbonate-to-matrix ratio with age approached significance in DT mice (25% increase, $P = 0.050$). These results indicate that bone tissue in DT mice is more immature than that in WT mice. In addition, while WT tissue matured as the mice aged, DT mice retained their immature tissue composition.

FTIR Spectroscopy—Repeatability

Mean CV values were calculated to assess repeatability of the FTIR measurements. Mean CV for FTIR measures ranged from 0.3% to 3.9%, with crystallinity displaying the lowest variation and carbonate-to-phosphate ratio displaying the highest variation for the samples tested (Table 2).

SRμCT Imaging

SRμCT data were evaluated to assess bone microstructure and TMD. Synchrotron imaging revealed dramatic differences in structure between WT and DT femora (Fig. 4). The 3-week-old DT femur had no distinct marrow cavity or cortical shell but, rather, a disorganized trabecular pattern throughout the cross section. This structural abnormality persisted in the 9-week-old DT femur. Quantitative analysis of the synchrotron data revealed differences in TMD mean and variance values. TMD values were 1,156 ± 100 and 711 ± 251 mg/cm^3 (mean ± SD) in WT and DT femur diaphyses, respectively, at 3 weeks and 1,205 ± 72 and 813 ± 133 mg/cm^3 in WT and DT mice, respectively, at 9 weeks. These results show that tissue composition and organization are altered in DT mice.

DXA Analysis

Whole-body BMD values were measured for DT and WT mice at 3, 6, 9, and 15 weeks of age to evaluate skeletal growth over the range of ages assessed via FTIR and SRμCT (Fig. 5). At 3 weeks of age DT mice had BMD values statistically indistinguishable from those of WT mice. BMD of DT mice was 103% that of their WT littermates by 6 weeks of age and 165% by 9 weeks ($P < 0.003$). BMD of DT mice remained constant through 15 weeks, with no statistically significant change detectable relative to the 9-week measurement. These results indicate that the accumulation of bone mineral in DT mice persists through sexual maturity, then plateaus in mature mice (>8 weeks).

Histology

Undecalcified sections were processed to visualize cortical and trabecular structure. Decalcified sections were stained

Table 1 FTIR analysis results for wild-type (WT) and double transgenic (DT) mice

	6-week animals			15-week animals		
	WT ($n = 6$)	DT ($n = 6$)	P	WT ($n = 6$)	DT ($n = 6$)	P
Phosphate:amide I	5.14 ± 0.68	3.85 ± 0.66	0.010	5.77 ± 0.83	4.10 ± 0.60	0.007
Carbonate:amide I	0.059 ± 0.007*	0.053 ± 0.006	0.084	0.088 ± 0.03*	0.066 ± 0.011	0.107
Carbonate:phosphate	0.012 ± 0.001*	0.014 ± 0.002	0.025	0.014 ± 0.001*	0.016 ± 0.001	0.006
Crystallinity 1,030/1,020	1.06 ± 0.01	1.02 ± 0.01	0.004	1.05 ± 0.01	1.02 ± 0.01	0.014
Cross-link ratio 1,660/1,690	1.73 ± 0.08*	1.54 ± 0.15	0.025	1.59 ± 0.11*	1.41 ± 0.06	0.010

Data for calvariae and femora were not different ($P > 0.05$); one mean value per animal was used for this analysis

* $P < 0.05$ by Wilcoxon rank sums test; all other 6- vs. 15-week comparisons, nonsignificant

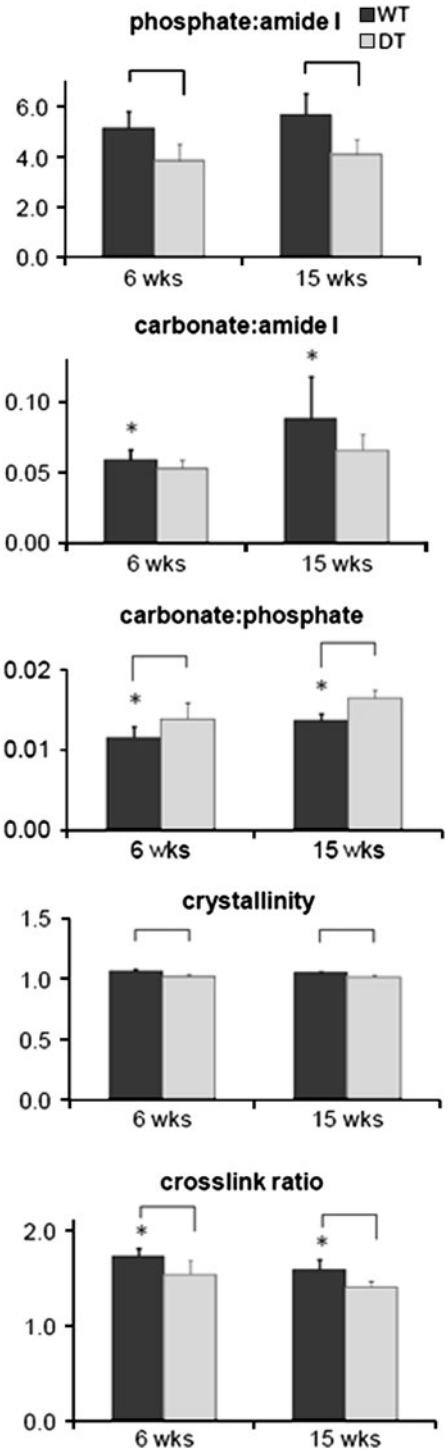

Fig. 3 FTIR spectroscopic results for 6- and 15-week wild-type (*WT*) and double transgenic (*DT*) mice. Significant variations from WT controls were evident in FTIR parameters describing mineral content, crystallinity, and collagen cross-links in DT bone at 6 weeks. These differences persisted in 15-week-old animals. As measurements for calvariae and femora were not different ($P > 0.05$), one mean value per animal was used for this analysis. *Bars* indicate significant differences between WT and DT animals (all $P < 0.03$). *Asterisks* indicate significant differences between 6- and 15-week animals (all $P < 0.05$)

with H&E to reveal cellular, matrix, and marrow components. A disordered mineralization pattern with effacement of the cortical compartment and elimination of the medullary canal was seen in these images (Fig. 6), in agreement with our previous finding that Rs1-induced basal G_s signaling in osteoblasts of DT mice increased trabecular bone and decreased cortical bone in lesions, reminiscent of fibrous dysplasia of the bone [6].

Discussion

Our results show that continuous G_s activation in mouse osteoblasts leads to deposition of large quantities of immature trabecular bone with reduced mineralization. FTIR spectroscopy revealed a 25–29% deficit in mineral-to-matrix ratio in the bones of mice expressing Rs1, and synchrotron imaging showed a reduced mean TMD. These findings are consistent with low levels of bone mineralization. Measures of mineral composition, mineral maturity, and collagen maturity also indicate significant abnormalities in bone formation induced by G_s activation in maturing osteoblasts. These alterations in tissue quality accompany dramatic structural changes, including greatly increased bone mass, increased heterogeneity of mineralization, disorganization of trabecular morphology, effacement of the cortical shell, and elimination of the medullary canal.

Our model is particularly relevant for GPCR diseases found in humans, including primary hyperparathyroidism and fibrous dysplasia of the bone such as that occurring in McCune-Albright syndrome. Patients with primary hyperparathyroidism present with marked cortical thinning and decreased cortical BMD [30, 31], possibly related to increased cortical porosity [32–34]. The elimination of the cortical compartment in DT mice is an extreme version of the cortical loss seen in primary hyperparathyroidism. However, the massive increase in trabecular volume observed in DT mice is not generally seen in patients with hyperparathyroidism. Bone from McCune-Albright syndrome patients shows a fibrous infiltrate, significant increases in trabecular bone formation, ablation of the marrow cavity, and an increased propensity to deformation and fracture [35]. In addition, these patients accumulate unmineralized osteoid with a nonlamellar structure as well as mineralized tissue with markedly reduced mineral content [1, 36]. The mineralization abnormalities found in our mouse model of fibrous dysplasia may reflect those in patients with fibrous dysplasia of the bone.

FTIR spectroscopic measures provide bone tissue characterization at the molecular level and, importantly, are correlated with mechanical integrity and remodeling properties of the tissue. Mineral-to-matrix ratio increases as

Table 2 Repeatability of FTIR spectroscopic parameters

	Phosphate:amide I	Carbonate:amide I	Carbonate:phosphate	Crystallinity 1,030/1,020	Cross-link ratio 1,660/1,690
Mean CV	1.15	3.46	3.86	0.32	1.72

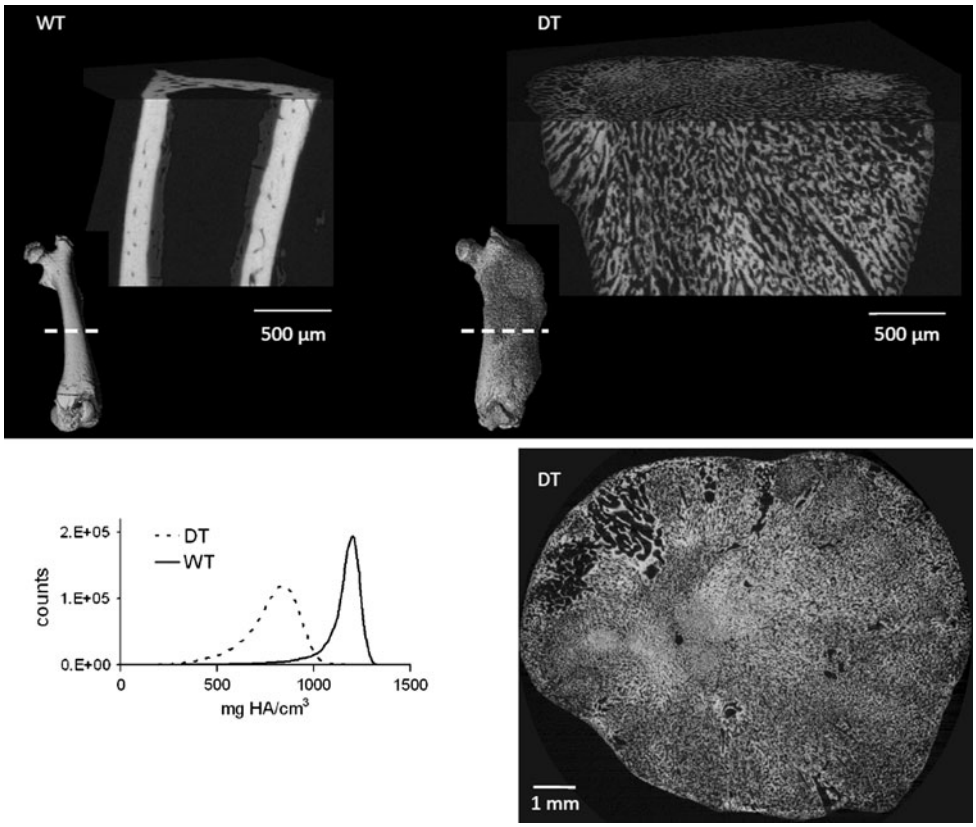

Fig. 4 Full bone renderings and detailed sections from the mid-diaphysis of femora from 3-week-old wild-type (*WT*) and double transgenic (*DT*) mice (*upper panel*). Mid-diaphyseal cross section of a 9-week-old DT mouse (*lower panel*). SRμCT images illustrate a disordered mineralization pattern, lack of dense cortical tissue, and elimination of central marrow cavity. Histograms compiled from synchrotron data of 3-week-old samples reveal decreased mean and increased variance in tissue mineral density in DT bone

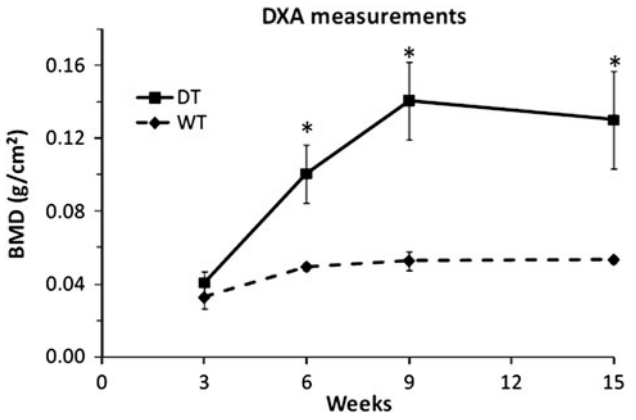

Fig. 5 BMD measured in age-matched wild-type (*WT*) and double transgenic (*DT*) littermates. Whole-body BMD values of DT mice were 103%, 165%, and 145% higher than those of WT littermate controls at 6, 9, and 15 weeks of age, respectively (*$P < 0.0003$ by *t*-test of DT vs. WT)

both primary and secondary mineralization progress and, therefore, is positively associated with tissue age [12, 37]. Studies of human tissue and animal models demonstrated positive correlations between mineral-to-matrix ratio and tissue stiffness and hardness [12, 38, 39]. Mineral-to-matrix ratio explains 50–60% of the variation in both tissue modulus and hardness [37, 40]. In our study, decreased mineral-to-matrix ratio in DT bone suggests the presence of immature bone with reduced resistance to deformation. Since FTIR crystallinity values are positively associated with tissue age, tissue yield strength, and stiffness [12, 14, 37], the decreased crystallinity we observed in DT bone substantiates the presence of immature tissue with reduced mechanical properties. We previously showed that DT animals have markedly elevated bone-turnover markers; display irregular, punctate bone formation by von Kossa staining and double fluorescent labeling; and have increased numbers of TRAP-positive osteoclasts [6]. These characteristics support the conclusion that DT bone lesions contain regions with extremely high rates of bone formation and turnover, consistent with our findings of accumulated immature tissue.

Increased carbonate substitution has been associated with increased tissue age [12, 15, 41, 42], increased tissue

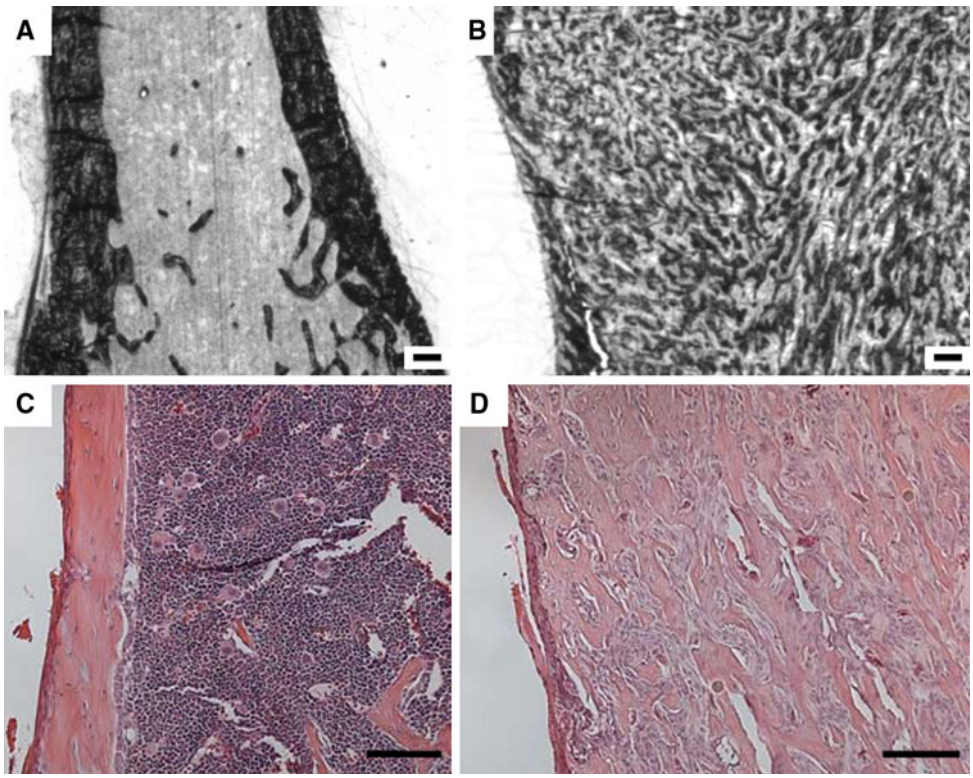

Fig. 6 Diaphyseal sections of representative 6-week-old wild-type (**a, c**) and double transgenic (**b, d**) femora visualized by microscopy. Undecalcified sections (**a, b**) and decalcified sections with H&E staining (**c, d**) demonstrate a disordered mineralization pattern with effacement of a distinct cortical compartment and elimination of the marrow canal in the double transgenic femur. *Scale bars* 1 mm

indentation modulus and hardness [40], and—by a mechanism of reduced ductility—increased incidence of fracture [43] and inferior mechanical properties at the whole-bone level [20]. Carbonate substitution in the hydroxyapatite lattice leads to a change in lattice dimensions and increased disorder of the crystalline structure [44]. Further, mineral solubility is affected by carbonate content and increased carbonate content is thought to enhance bone resorption [45]. Carbonate-to-phosphate ratio was significantly elevated in DT bone, indicating an alteration in crystal synthesis and perhaps playing a role in the high turnover observed in DT animals [6].

Collagen matrix biochemistry is also related to tissue age, mineralization, and mechanics. Intermolecular cross-linking provides the matrix tensile strength and influences whole-bone strength [46–49]. Cross-link formation also alters the rate of mineralization and microdamage accumulation [50], thereby providing a second mechanism for regulating the mechanical properties of bone [51]. The ratio of mature to immature, reducible cross-links—quantified as cross-link ratio—increases with tissue maturity [52, 53] and correlates positively with indentation modulus [12]. In DT bone, low cross-link ratio indicates immature tissue with reduced stiffness.

FTIR analyses showed that DT bone does not exhibit maturation between 6 and 15 weeks. In contrast, specimens from 6- and 15-week-old WT mice showed significant differences in carbonate-to-matrix and carbonate-to-phosphate ratios, indicative of increasingly mature tissue. Cross-link ratio decreased in WT animals, in contrast to the established association between cross-link ratio and matrix maturation.

SRμCT imaging was used to quantify mean TMD and distribution of TMD values, measures complementary to those determined through FTIR analysis. Consistent with the deficit in mineral-to-matrix ratio identified by FTIR, DT bone had mean TMD values 39% and 33% lower than WT bone at 3 and 9 weeks, respectively. SRμCT also revealed increased heterogeneity in mineral content in DT mice as reflected by the large standard deviation of TMD in DT bones at 3 and 9 weeks (151% and 88% higher, respectively). The alteration in distribution of mineralization values might significantly affect the overall material properties of DT bone; heterogeneous regions of tissue mineralization may hinder crack propagation and toughen tissue. It is intriguing to consider that the increased variation in TMD may represent a compensatory mechanism by which DT mice counteract the deficit in tissue mineralization. Increased tissue volume in DT animals may represent an additional adaptive response to the formation of hypomineralized tissue and loss of cortical structure. These changes may partially or fully compensate for any loss of whole-bone strength or stiffness. No spontaneous fractures have been identified in DT animals, perhaps supporting this hypothesis.

The presence of immature bone in our mouse model of fibrous dysplasia suggests that strategies for modulating

bone formation, such as antiresorptive medications, may have therapeutic value for these patients. Since the fibrous dysplastic bone lesions appear to be reversible by inhibiting G_s signaling [54], the immature bone formation seen in our DT mice might also be reversed. This would be an important metric as potential therapies for fibrous dysplasia are developed.

Despite identifying significant effects of Rs1 signaling on bone mineralization, our study has several limitations. First, we were unable to perform direct measurement of mechanical competence in DT mice. Mechanical testing is challenging in DT specimens due to morphological abnormalities and heterogeneous mineralization. However, the compositional measures derived from FTIR and SRμCT data are highly associated with mechanical properties of bone tissue and give us insight into the mechanisms of increased fragility in fibrous dysplastic bone. Second, the ages of animals characterized by FTIR and SRμCT were different; this should be taken into consideration when making direct comparisons between analysis results. However, for each analysis technique, the younger animals (3 and 6 weeks old) were in the rapid skeletal growth phase, while the older animals (9 and 15 weeks old) had reached a plateau of bone accumulation. This is supported by BMD measurements and consistent with the observed sexual maturity window of 7–8 weeks in both WT and DT mice. Finally, our findings are based on samples from a relatively small number of animals. The significant abnormalities in tissue quality and skeletal structure we observed in our TD mice were surprisingly conserved between the two different anatomic sites sampled (femora and parietal bones of calvariae). This finding allowed us to compile results from the two skeletal sites and perform a conservative statistical analysis. Despite these limitations, we believe that our results provide new insight into the roles of G_s signaling in regulating the matrix formation process.

In conclusion, our results illustrate that activation of the G_s signaling pathway in maturing osteoblasts leads to a significant degradation of bone tissue quality in a mouse model of fibrous dysplasia. The striking influence of the fibrous dysplasia model on tissue quality metrics reinforces the paradigm that tissue quality, and not just quantity and structure, must be considered in the evaluation of any disease processes or potential therapies.

Acknowledgments The authors thank Francoise Peyrin, PhD, the scientists of ESRF beamline ID19, and Andrew Burghardt for assistant with synchrotron imaging as well as Joyce Pang for assistance with specimen processing. This study was funded by NIH F32-AR053446 (to G. J. K.); NIH K08 AR056299-02 (to E. C. H.); the France-Berkeley Fund (to S. M.); NIH R01-HL60664 (to B. R. C.); the VA Merit Review Fund and NIH RO1-DK072071 (to R. A. N.). We also thank Mark Scott, Gary Howard, and the Gladstone Histology Core for valuable technical assistance and discussions. The J. David Gladstone Institutes received support from a National Center for Research Resources Grant (RR18928-01).

References

1. Chapurlat RD, Orcel P (2008) Fibrous dysplasia of bone and McCune-Albright syndrome. Best Pract Res Clin Rheumatol 22:55–69
2. Weinstein LS (2006) G_s alpha mutations in fibrous dysplasia and McCune-Albright syndrome. J Bone Miner Res 21(Suppl 2): P120–P124
3. Dobnig H, Turner RT (1997) The effects of programmed administration of human parathyroid hormone fragment (1–34) on bone histomorphometry and serum chemistry in rats. Endocrinology 138:4607–4612
4. Conklin BR, Hsiao EC, Claeysen S, Dumuis A, Srinivasan S, Forsayeth JR, Guettier JM, Chang WC, Pei Y, McCarthy KD, Nissenson RA, Wess J, Bockaert J, Roth BL (2008) Engineering GPCR signaling pathways with RASSLs. Nat Methods 5: 673–678
5. Chang WC, Ng JK, Nguyen T, Pellissier L, Claeysen S, Hsiao EC, Conklin BR (2007) Modifying ligand-induced and constitutive signaling of the human 5-HT4 receptor. PLoS One 2:e1317
6. Hsiao EC, Boudignon BM, Chang WC, Bencsik M, Peng J, Nguyen TD, Manalac C, Halloran BP, Conklin BR, Nissenson RA (2008) Osteoblast expression of an engineered G_s-coupled receptor dramatically increases bone mass. Proc Natl Acad Sci USA 105:1209–1214
7. Redfern CH, Coward P, Degtyarev MY, Lee EK, Kwa AT, Hennighausen L, Bujard H, Fishman GI, Conklin BR (1999) Conditional expression and signaling of a specifically designed G_i-coupled receptor in transgenic mice. Nat Biotechnol 17: 165–169
8. Scearce-Levie K, Lieberman MD, Elliott HH, Conklin BR (2005) Engineered G protein coupled receptors reveal independent regulation of internalization, desensitization and acute signaling. BMC Biol 3:3
9. Sweger EJ, Casper KB, Scearce-Levie K, Conklin BR, McCarthy KD (2007) Development of hydrocephalus in mice expressing the G_i-coupled GPCR Ro1 RASSL receptor in astrocytes. J Neurosci 27:2309–2317
10. Zhao GM, Qian X, Schiller PW, Szeto HH (2003) Comparison of [Dmt1]DALDA and DAMGO in binding and G protein activation at mu, delta, and kappa opioid receptors. J Pharmacol Exp Ther 307:947–954
11. Boyce TM, Bloebaum RD (1993) Cortical aging differences and fracture implications for the human femoral neck. Bone 14: 769–778
12. Gourion-Arsiquaud S, Faibish D, Myers E, Spevak L, Compston J, Hodsman A, Shane E, Recker RR, Boskey ER, Boskey AL (2009) Use of FTIR spectroscopic imaging to identify parameters associated with fragility fracture. J Bone Miner Res 24: 1565–1571
13. Rho JY, Zioupos P, Currey JD, Pharr GM (1999) Variations in the individual thick lamellar properties within osteons by nanoindentation. Bone 25:295–300
14. Yerramshetty JS, Akkus O (2008) The associations between mineral crystallinity and the mechanical properties of human cortical bone. Bone 42:476–482
15. Boskey AL, Young MF, Kilts T, Verdelis K (2005) Variation in mineral properties in normal and mutant bones and teeth. Cells Tissues Organs 181:144–153

16. Doi Y, Iwanaga H, Shibutani T, Moriwaki Y, Iwayama Y (1999) Osteoclastic responses to various calcium phosphates in cell cultures. J Biomed Mater Res 47:424–433
17. Boskey AL, Mendelsohn R (2005) Infrared spectroscopic characterization of mineralized tissues. Vib Spectrosc 38:107–114
18. Miller LM, Vairavamurthy V, Chance MR, Mendelsohn R, Paschalis EP, Betts F, Boskey AL (2001) In situ analysis of mineral content and crystallinity in bone using infrared micro-spectroscopy of the nu(4) PO(4)(3-) vibration. Biochim Biophys Acta 1527:11–19
19. Faibish D, Gomes A, Boivin G, Binderman I, Boskey A (2005) Infrared imaging of calcified tissue in bone biopsies from adults with osteomalacia. Bone 36:6–12
20. Pienkowski D, Doers TM, Monier-Faugere MC, Geng Z, Camacho NP, Boskey AL, Malluche HH (1997) Calcitonin alters bone quality in beagle dogs. J Bone Miner Res 12:1936–1943
21. Rey C, Renugopalakrishnan V, Collins B, Glimcher MJ (1991) Fourier transform infrared spectroscopic study of the carbonate ions in bone mineral during aging. Calcif Tissue Int 49:251–258
22. Gadaleta SJ, Paschalis EP, Betts F, Mendelsohn R, Boskey AL (1996) Fourier transform infrared spectroscopy of the solution-mediated conversion of amorphous calcium phosphate to hydroxyapatite: new correlations between X-ray diffraction and infrared data. Calcif Tissue Int 58:9–16
23. Pleshko N, Boskey A, Mendelsohn R (1991) Novel infrared spectroscopic method for the determination of crystallinity of hydroxyapatite minerals. Biophys J 60:786–793
24. Paschalis EP, Verdelis K, Doty SB, Boskey AL, Mendelsohn R, Yamauchi M (2001) Spectroscopic characterization of collagen cross-links in bone. J Bone Miner Res 16:1821–1828
25. Kazakia GJ, Burghardt AJ, Cheung S, Majumdar S (2008) Assessment of bone tissue mineralization by conventional X-ray microcomputed tomography: comparison with synchrotron radiation microcomputed tomography and ash measurements. Med Phys 35:3170–3179
26. Nuzzo S, Peyrin F, Cloetens P, Baruchel J, Boivin G (2002) Quantification of the degree of mineralization of bone in three dimensions using synchrotron radiation microtomography. Med Phys 29:2672–2681
27. Peng J, Bencsik M, Louie A, Lu W, Millard S, Nguyen P, Burghardt A, Majumdar S, Wronski TJ, Halloran B, Conklin BR, Nissenson RA (2008) Conditional expression of a G_i-coupled receptor in osteoblasts results in trabecular osteopenia. Endocrinology 149:1329–1337
28. Peyrin F, Muller C, Carillon Y, Nuzzo S, Bonnassie A, Briguet A (2001) Synchrotron radiation microCT: a reference tool for the characterization of bone samples. Adv Exp Med Biol 496: 129–142
29. Burghardt AJ, Kazakia GJ, Majumdar S (2007) A local adaptive threshold strategy for high resolution peripheral quantitative computed tomography of trabecular bone. Ann Biomed Eng 35:1678–1686
30. Charopoulos I, Tournis S, Trovas G, Raptou P, Kaldrymides P, Skarandavos G, Katsalira K, Lyritis GP (2006) Effect of primary hyperparathyroidism on volumetric bone mineral density and bone geometry assessed by peripheral quantitative computed tomography in postmenopausal women. J Clin Endocrinol Metab 91:1748–1753
31. Hansen S, Jensen JE, Rasmussen L, Hauge EM, Brixen K (2010) Effects on bone geometry, density and microarchitecture in the distal radius but not tibia in women with primary hyperparathyroidism. A case-control study using HR-pQCT. J Bone Miner Res 25:1941–1947
32. Christiansen P, Steiniche T, Brockstedt H, Mosekilde L, Hessov I, Melsen F (1993) Primary hyperparathyroidism: iliac crest cortical thickness, structure, and remodeling evaluated by histomorphometric methods. Bone 14:755–762
33. Eriksen EF (2002) Primary hyperparathyroidism: lessons from bone histomorphometry. J Bone Miner Res 17(Suppl 2):N95–N97
34. Parisien M, Silverberg SJ, Shane E, de la Cruz L, Lindsay R, Bilezikian JP, Dempster DW (1990) The histomorphometry of bone in primary hyperparathyroidism: preservation of cancellous bone structure. J Clin Endocrinol Metab 70:930–938
35. O'Sullivan M, Zacharin M (2002) Intramedullary rodding and bisphosphonate treatment of polyostotic fibrous dysplasia associated with the McCune-Albright syndrome. J Pediatr Orthop 22:255–260
36. Corsi A, Collins MT, Riminucci M, Howell PG, Boyde A, Robey PG, Bianco P (2003) Osteomalacic and hyperparathyroid changes in fibrous dysplasia of bone: core biopsy studies and clinical correlations. J Bone Miner Res 18:1235–1246
37. Miller LM, Little W, Schirmer A, Sheik F, Busa B, Judex S (2007) Accretion of bone quantity and quality in the developing mouse skeleton. J Bone Miner Res 22:1037–1045
38. Camacho NP, Rimnac CM, Meyer RA Jr, Doty S, Boskey AL (1995) Effect of abnormal mineralization on the mechanical behavior of X-linked hypophosphatemic mice femora. Bone 17:271–278
39. Courtland HW, Nasser P, Goldstone AB, Spevak L, Boskey AL, Jepsen KJ (2008) Fourier transform infrared imaging microspectroscopy and tissue-level mechanical testing reveal intra-species variation in mouse bone mineral and matrix composition. Calcif Tissue Int 83:342–353
40. Donnelly E, Chen DX, Boskey AL, Baker SP, van der Meulen MC (2010) Contribution of mineral to bone structural behavior and tissue mechanical properties. Calcif Tissue Int 87:450–460
41. Donnelly E, Boskey AL, Baker SP, van der Meulen MC (2010) Effects of tissue age on bone tissue material composition and nanomechanical properties in the rat cortex. J Biomed Mater Res A 92:1048–1056
42. Tarnowski CP, Ignelzi MA Jr, Morris MD (2002) Mineralization of developing mouse calvaria as revealed by Raman microspectroscopy. J Bone Miner Res 17:1118–1126
43. McCreadie BR, Morris MD, Chen TC, Sudhaker Rao D, Finney WF, Widjaja E, Goldstein SA (2006) Bone tissue compositional differences in women with and without osteoporotic fracture. Bone 39:1190–1195
44. Zapanta-LeGeros R (1965) Effect of carbonate on the lattice parameters of apatite. Nature 206:403–404
45. Spence G, Patel N, Brooks R, Bonfield W, Rushton N (2010) Osteoclastogenesis on hydroxyapatite ceramics: the effect of carbonate substitution. J Biomed Mater Res A 92:1292–1300
46. Banse X, Sims TJ, Bailey AJ (2002) Mechanical properties of adult vertebral cancellous bone: correlation with collagen intermolecular cross-links. J Bone Miner Res 17:1621–1628
47. Knott L, Whitehead CC, Fleming RH, Bailey AJ (1995) Biochemical changes in the collagenous matrix of osteoporotic avian bone. Biochem J 310:1045–1051
48. Oxlund H, Barckman M, Ortoft G, Andreassen TT (1995) Reduced concentrations of collagen cross-links are associated with reduced strength of bone. Bone 17:365S–371S
49. Yamauchi M, Young DR, Chandler GS, Mechanic GL (1988) Cross-linking and new bone collagen synthesis in immobilized and recovering primate osteoporosis. Bone 9:415–418
50. Zoehrer R, Dempster DW, Bilezikian JP, Zhou H, Silverberg SJ, Shane E, Roschger P, Paschalis EP, Klaushofer K (2008) Bone quality determined by Fourier transform infrared imaging analysis in mild primary hyperparathyroidism. J Clin Endocrinol Metab 93:3484–3489

51. Saito M, Marumo K (2010) Collagen cross-links as a determinant of bone quality: a possible explanation for bone fragility in aging, osteoporosis, and diabetes mellitus. Osteoporos Int 21:195–214
52. Eyre DR, Dickson IR, Van Ness K (1988) Collagen cross-linking in human bone and articular cartilage. Age-related changes in the content of mature hydroxypyridinium residues. Biochem J 252: 495–500
53. Paschalis EP, Recker R, DiCarlo E, Doty SB, Atti E, Boskey AL (2003) Distribution of collagen cross-links in normal human trabecular bone. J Bone Miner Res 18:1942–1946
54. Hsiao EC, Boudignon BM, Halloran BP, Nissenson RA, Conklin BR (2010) G_s G protein–coupled receptor signaling in osteoblasts elicits age-dependent effects on bone formation. J Bone Miner Res 25:584–593